JOURNAL OF MATERIALS SCIENCE 27 (1992) 2719–2725

Dislocations and grain boundaries in polycrystalline ice: a preliminary study by synchrotron X-ray topography

F. LIU, I. BAKER
Thayer School of Engineering, Dartmouth College, Hanover, NH 03755, USA
G. YAO, M. DUDLEY
Department of Materials Science, State University of New York at Stony Brook, Stony Brook, NY 11794, USA

White-beam synchrotron X-ray topography has been used to image dislocations and grain boundaries in high-purity columnar-grained polycrystalline ice. It was found that screw, 30° and 60° basal dislocations with $< 1\,1\,\bar{2}\,0 >$ Burgers vectors far outnumber other dislocations: near free surfaces, the dislocations were bent because of image forces. Circular prismatic dislocation loops with [0 0 0 1] Burgers vectors and dipoles were also found. These probably formed due to thermal shock. In one sample, the dislocation structures of three grains were clearly observed simultaneously, although no dislocations were visible in the boundaries.

1. Introduction

X-ray topography has been extensively used to study dislocations in single-crystal ice [1] because of its non-destructive character, i.e. the specimens do not suffer any radiation damage even after repeatedly taking topographs. The low X-ray absorption coefficient and low dislocation density ($< 10^2\ cm^{-2}$) in ice make individual dislocations easily discernable even in crystals of a few millimetres thick. In recent years, the power of the technique has been greatly enhanced by the use of X-rays from a synchrotron radiation source [2–6].

Naturally, ice exists not as single crystals but as polycrystals. Various phenomena such as creep, yielding, fracture, and obviously grain growth, depend on the presence of grain boundaries in addition to the lattice processes. Compared with grain-boundary studies in metals, the study of grain boundaries in ice is immature. Some efforts have been made to study grain boundaries in bicrystal ice with the Lang method using conventional X-ray sources [7–9]. However, the *in situ* images were blurred because of the long exposure times required. Thus far, all bicrystals studied by X-ray topography have been grown by adjusting two seed crystals as close as possible to the misorientation predicted by the coincidence-site lattice (CSL) model. However, this is quite different from the way most polycrystalline ice occurs naturally.

Since grain boundaries do not absorb X-rays more than the lattice in ice [10], the synchrotron-based Laue technique can be used to study both grain boundaries and dislocations in polycrystalline ice. The high intensity and high collimation of synchrotron radiation can be used to reveal the interaction mechanism between dislocations and grain boundaries. Thus far, this technique has not been used to study polycrystalline ice. A description is given of the successful application of this technique to observe grain boundaries and dislocations in "pure" polycrystalline ice. A significant feature of our observations is that the dislocation structures from both sides of each boundary were observed simultaneously on one X-ray film with exposure times of about 2 s. These preliminary observations have established the feasibility of our ongoing work: to examine the interaction mechanism between dislocations and grain boundaries in ice.

2. Sample preparation

The polycrystalline ice with columnar grains used in these experiments was grown, from water that had been purified and de-gassed, using a seedless Czochralski method. The samples were cut initially with a band-saw and then with a fine jeweller's saw into rectangular blocks. The crystallographic orientation of each grain was identified initially by the shape of etch pits [11]. The positions of grain boundaries were determined by viewing samples between crossed polarized sheets. The rectangular ice sample was planed roughly to 3 mm thickness and the required area of a few centimetres length and width by gently shaving the sample with a razor [3]. Then the surface was carefully removed by polishing it with a smooth cloth soaked in ethyl alcohol until its thickness was reduced to ~ 2 mm [1]. The alcohol adhering to the specimen surface was removed by washing the sample in a normal hexane bath. The final specimens, measuring 25 mm × 15 mm × 2 mm, were mounted on a PEEK base, which has the same linear thermal

0022–2461

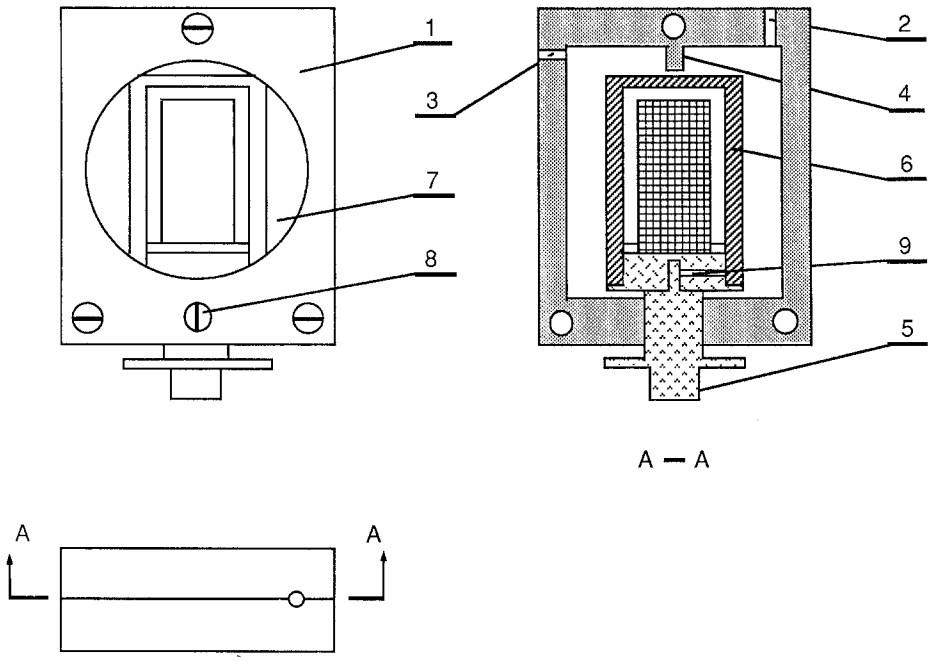

Figure 1 The cryostat used in the preliminary study: (1) strengthened Plexiglass frame, (2) cold nitrogen gas inlet, (3) cold nitrogen gas exit, (4) protrusion to prevent nitrogen gas flowing out without circulation, (5) nylon rod to fit on synchrotron goniometer stage, (6) inner chamber (see Fig. 2), (7) five-layer Melinex windows, transparent to X-rays, (8) screw to close the cryostat, (9) screw to fix the nylon rod to the PEEK base.

expansion coefficient. They were annealed at $-10\,^{\circ}C$ for 15 days. Note that damage, which always occurs at the mount, does not anneal out. For examination, the specimens were cooled down to $-20\,^{\circ}C$ very slowly, and transported to the National Synchrotron Light Source, Brookhaven National Laboratory, New York, where the specimens were transferred to a specially built cryostat.

3. Set-up and testing procedures

The cryostat, shown in Fig. 1, had multi-layer Melinex windows transparent to X-rays, and was mounted on a goniometer with the synchrotron radiation beam passing through the large faces of the sample [12]. In order to prevent sublimation, the sample is sealed inside a nylon chamber with single-layer windows, as shown in Fig. 2. The sample was cooled with nitrogen gas which had been bubbled through liquid nitrogen. The temperature, $-18.5^{\circ} \pm 0.5\,^{\circ}C$, was controlled within the cryostat by controlling the nitrogen gas flow rate. An aluminium filter was used to absorb long wavelengths in the X-ray spectrum which would damage the sample. The direct beam was stopped by a piece of lead to prevent blurring of the X-ray film. All experiments were carried out at 2.5 GeV, 200 mA, with exposure times of about 2 s. No evidence of radiation damage was found.

Several sets of transmission Laue patterns were recorded on a high-resolution X-ray film placed 10 cm from the sample and perpendicular to the incident beam. Each Laue diffraction spot so formed is a two-dimensional projection of the three-dimensional defect structure in the specimen: suitable rotations of the sample can be used to separate any overlapping diffraction spots. The chosen diffraction plane can be achieved by adjusting the goniometer head on which

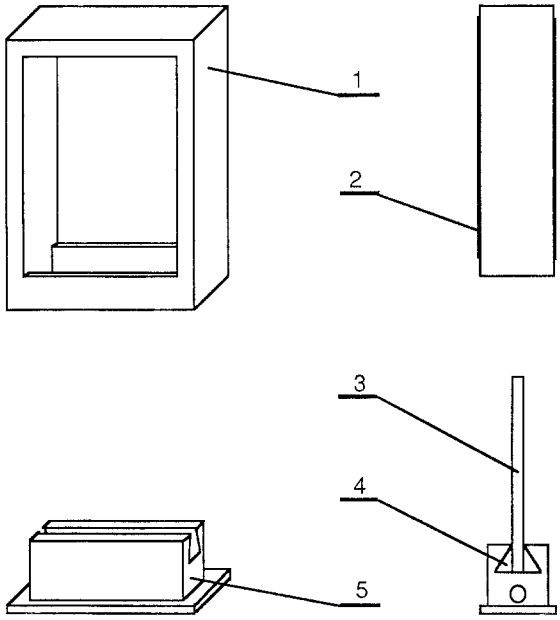

Figure 2 The inner chamber used to prevent ice sublimation and thermal shock: (1) PEEK frame, (2) single-layer Melinex window, (3) polycrystalline ice sample, (4) frozen water, (5) PEEK base.

the specimen is fixed. The sample is shifted up and down relative to the beam in order to obtain topographs of the whole sample. From the shape of a diffraction spot, its corresponding grain can be identified. Combining the orientation information revealed by the shape of etch pits with the transmission Laue patterns, the incident beam direction was calculated and all Laue patterns were indexed using a computer program. The crystal was exposed to the X-rays only during the taking of a topograph.

In order to reveal the complete dislocation structure, several diffraction patterns were taken from each

region of the sample. The relative distance between and shape changes of any two dislocations in different diffraction images were used to determine the three-dimensional character of the dislocations.

4. Results and discussion

Fig. 3 shows typical dislocation structures of the same area inside one large grain, with the broadest surfaces on basal planes. The topographs of Fig. 3a, b and c are $(1\,0\,\bar{1}\,0)$, $(0\,\bar{1}\,1\,0)$ and $(\bar{1}\,1\,0\,0)$ images, respectively. The diffraction vector $\boldsymbol{g}$ is shown on an attached hexagonal figure, whose corners correspond to the various directions like $[1\,1\,\bar{2}\,0]$, $[1\,\bar{2}\,1\,0]$, $[\bar{2}\,1\,1\,0]$, etc. The hexagon has the same shape as the etch pit. In order to determine the Burgers vector $\boldsymbol{b}$, the following invisibility criteria were used; $\boldsymbol{g}\cdot\boldsymbol{b}=0$ for screw dislocations, and both $\boldsymbol{g}\cdot\boldsymbol{b}=0$ and $\boldsymbol{g}\cdot\boldsymbol{b}\times\boldsymbol{u}=0$ for edge dislocations, where $\boldsymbol{u}$ is the line vector of the dislocation. In this case, six topographs taken with three different diffraction vectors of $<1\,0\,\bar{1}\,0>$ and of $<1\,1\,\bar{2}\,0>$ were used. It was found that the dislocations lie in the basal plane. It is hard to see any segments which look like connecting dislocations lying on different parallel basal planes without careful analyses. Burgers vector analyses showed that screw, 30° and 60° dislocations with Burgers vectors of $<1\,1\,\bar{2}\,0>$ type, lying on basal planes, outnumber other kinds of dislocations. No stacking faults were observed.

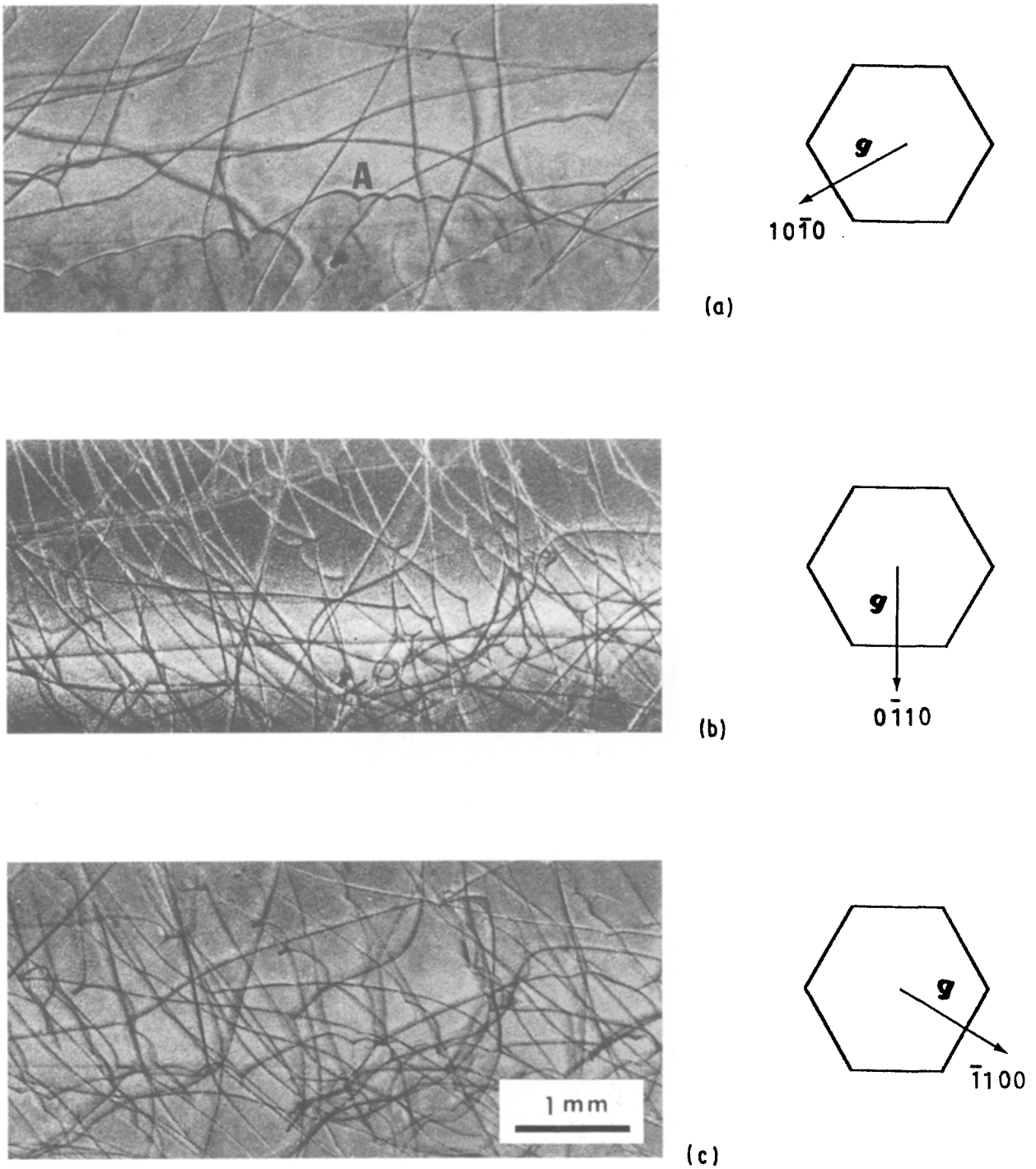

Figure 3 A typical dislocation structure in a large grain: (a) $(1\,0\,\bar{1}\,0)$ image, $\lambda = 0.069$ nm; (b) $(0\,\bar{1}\,1\,0)$ image, $\lambda = 0.081$ nm; (c) $(\bar{1}\,1\,0\,0)$ image, $\lambda = 0.069$ nm.

An important feature is the cusp-shaped dislocations, like the one marked A in Fig. 3a. This particular dislocation, similar to one studied previously [13], is composed of edge-dislocation dipoles generated from the pre-existing screw dislocation with the same Burgers vector $[\bar{2}\,1\,1\,0]$ during very slow cooling from -10 to $-20\,^{\circ}C$. During the cooling, an extra half-plane was inserted by point defect condensation, i.e. by a climbing motion of the edge superjog which connected the screw dislocations on different basal planes.

Fig. 4 shows the dislocation structures near a free surface. Figs 4a, b, c and d are images from $(0\,1\,\bar{1}\,0)$, $(\bar{1}\,1\,0\,0)$, $(2\,\bar{1}\,\bar{1}\,0)$ and $(1\,0\,\bar{1}\,0)$ reflections, respectively. All dislocations were visible for the $(2\,\bar{1}\,\bar{1}\,0)$ reflection, indicating that none had Burgers vectors in the $(2\,\bar{1}\,\bar{1}\,0)$ plane. Where the basal dislocations, marked B, C, D and E, emerge on the free surface, which is nearly

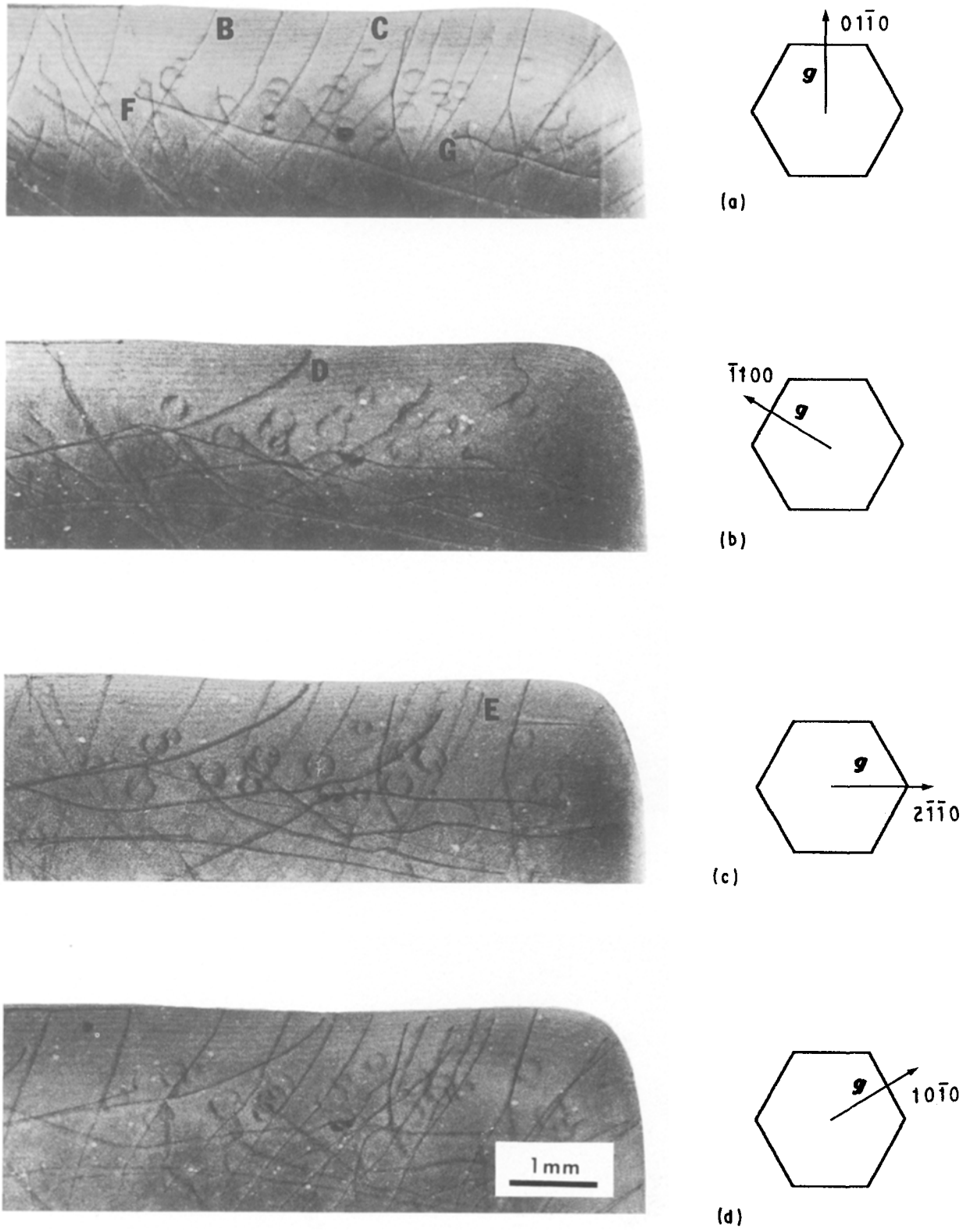

Figure 4 The dislocation structure near a free surface, showing the dislocations bending due to image forces: (a) $(0\,1\,\bar{1}\,0)$ image, $\lambda = 0.091$ nm; (b) $(\bar{1}\,1\,0\,0)$ image, $\lambda = 0.081$ nm; (c) $(2\,\bar{1}\,\bar{1}\,0)$ image, $\lambda = 0.069$ nm; (d) $(1\,0\,\bar{1}\,0)$ image, $\lambda = 0.093$ nm.

perpendicular to basal planes, they bend due to image forces, i.e. in order to minimize energy. Where the two long 30° $[1\bar{2}10]$ dislocations, marked F and G, emerge on the broadest surface of the specimen, they are bent and have formed superjogs on the non-basal planes. The superjogs showed no tendency to take up any special orientations. This is a common feature in this sample and in many of the other samples, especially when the free surface had an oblique intersection with the basal planes. It is not straightforward to determine the planes on which the dislocations lie, owing to the possible unevenness of the surface and peculiarities of the dislocation images near the surface, as well as owing to the possible shift via superjogs from one basal plane to another along the dislocations. The approximate edge orientations were clearly irregular and might have segments on various planes.

This sample underwent some thermal shock when it was transferred to the cryostat, i.e. from -20 to $-8\,^{\circ}C$ and then to $-18\,^{\circ}C$ within several minutes. This produced a number of prismatic loops in regions of very low dislocation density, shown in Fig. 4. Self-interstitials of water molecules are common, at least in the temperature range between 0 and $-50\,^{\circ}C$ [14]. Thus, these dislocation loops were probably formed by the condensation of interstitials. All the dislocation loops are on the basal plane, and are invisible where $\boldsymbol{g}\cdot\boldsymbol{b}\times\boldsymbol{u}=0$ and $\boldsymbol{g}\cdot\boldsymbol{b}=0$, indicating that these dislocation loops have an [0001] Burgers vector.

Fig. 5 shows a schematic sketch of an ice sample with three columnar grains. The two broadest surfaces are (0001) planes for grain 3. The misorientation between grain 2 and grain 3 is plotted in Fig. 6. The orientation of grain 1 was not determined because of the difficulties involved in etching such a small grain. Also, the limited number of diffraction spots from this grain in the transmission Laue pattern were not enough for orientation determination.

Fig. 7a shows the dislocation structures in grain 1. It was clear that the sharp edge of the sample had been removed by chemical polishing. According to the Bragg law, the X-ray spectrum and the intensity of this diffraction spot relative to others, it must be the diffraction from the $(10\bar{1}0)$ plane and, hence, has a corresponding wavelength of 0.069 nm. In the right of grain 1, several loops are visible. They are, most probably, images of dislocation circular loops with a [0001] Burgers vector, cut by the surface of the specimen. It is interesting that the partial loops were connected together by dislocation climb motion, and are most probably again on the same basal plane. Near the middle of the grain, some impurities, probably air bubbles, distributed along the growth direction, are present.

The dislocations in grain 2 are shown in Fig. 7b which was taken immediately after the sample was transferred into the cryostat. Fig. 7c is the image from the same plane $(\bar{1}100)$, but taken about 10 min later. A temperature slightly higher than $-18.5\,^{\circ}C$ was used to transfer the sample. The dislocation structure was similar to that in Fig. 3. The two topographs show the expansion of a pre-existing prismatic loop, marked H, and the nucleation of a new loop. Since a cooling

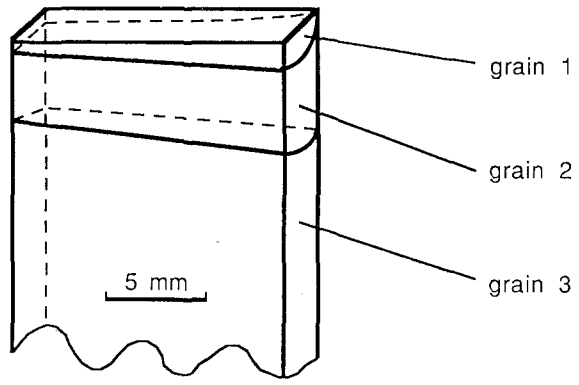

Figure 5 A schematic sketch of an ice sample containing three columnar grains.

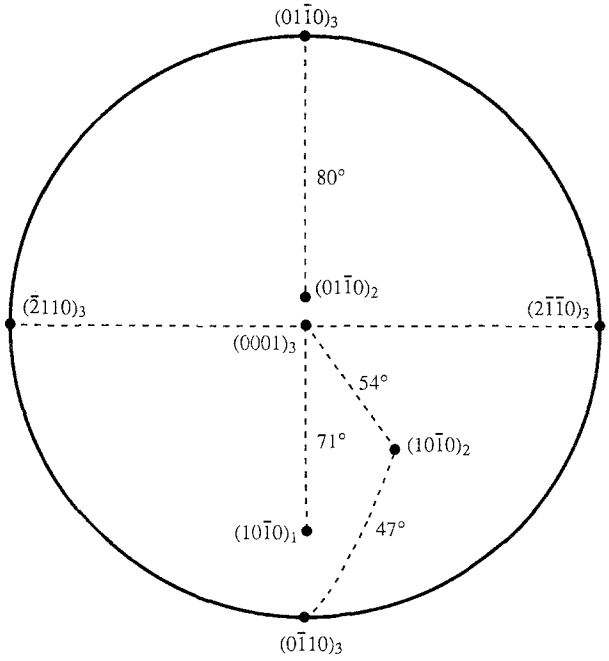

Figure 6 Stereographic projection showing the misorientation between grain 2 and grain 3 shown in Fig. 5.

rate of $2\,^{\circ}C\ h^{-1}$ is enough to cause the condensation of excess interstitials [1], the expansion and nucleation of dislocation loops is a result of interactions of the pre-existing dislocation loop with point defects. This is a process of edge-dislocation climb caused by absorption or release of interstitials. The dislocation loops would bulge out one by one as long as the diffusion of excess interstitials continued.

Fig. 7d shows the dislocations in grain 3, in a $(0\bar{1}10)$ image, corresponding to a wavelength of 0.077 nm. A feature worth noting is that no long screw dislocations with line directions parallel to the growth direction are present. This suggests a layer growth mechanism in the case of growing columnar grains with the seedless Czochralski method, and not growth around screw dislocations.

The four topographs in Fig. 7 show the two large-angle grain boundaries between grains 1 and 2 and grains 2 and 3. Pendellösung fringes appeared as wide horizontal lines along the grain boundaries. The dislocation density in each grain is sufficiently low

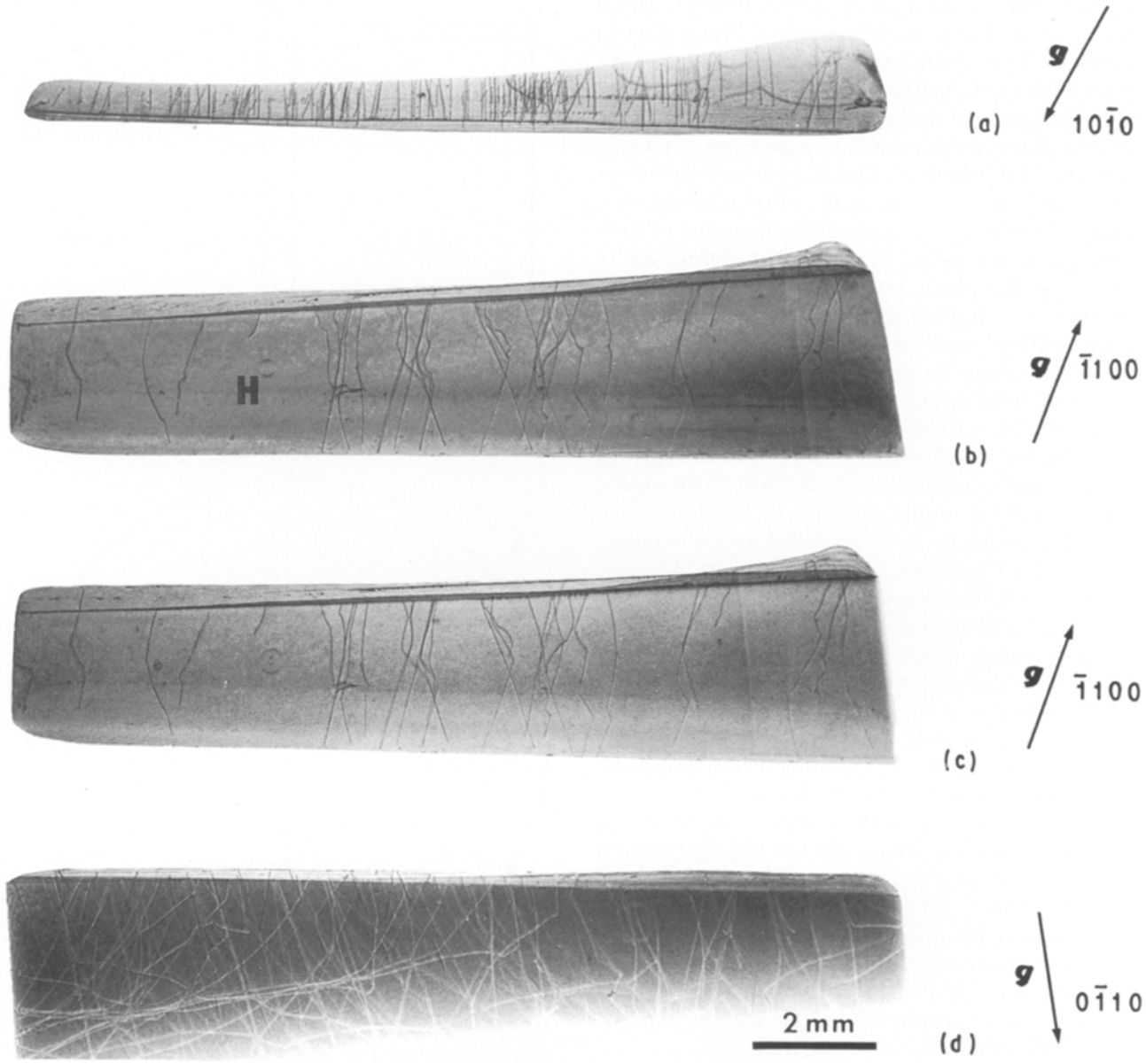

Figure 7 X-ray topographs showing two grain boundaries in one sample: (a) (1 0 $\bar{1}$ 0) image from grain 1, $\lambda = 0.069$ nm; (b) ($\bar{1}$ 1 0 0) image from grain 2, $\lambda = 0.095$ nm; (c) ($\bar{1}$ 1 0 0) image from grain 2, $\lambda = 0.095$ nm, taken about 10 min after (b); and (d) (0 $\bar{1}$ 1 0) image from grain 3, $\lambda = 0.077$ nm.

($< 10^5$ m^{-2}), to allow observation of the boundaries themselves. Since X-ray diffraction is quite sensitive to any strain field, the absence of line images on or near the boundaries means that either there were no stress concentrations, or if present, they were relaxed after long annealing. No long-range stress field was exerted by the equilibrium grain boundaries. Neither grain boundary facets nor dislocations within the grain boundaries were observed in our study.

5. Conclusions

Examination of high-purity columnar-grained polycrystalline ice samples using a synchrotron-based Laue technique has led to the following conclusions.

1. Screw, 30° and 60° basal dislocations with $< 1\,1\,\bar{2}\,0 >$ Burgers vectors far outnumber other dislocations.

2. Dislocations near a free surface bend due to image forces.

3. Slow cooling produces dislocation dipoles.

4. Thermal shock results in the nucleation and expansion of prismatic dislocation loops.

5. There appears to be no long-range stress field on or near equilibrium grain boundaries to impede the examination of the interaction mechanism between dislocations and grain boundaries.

Acknowledgements

The authors wish to express their sincere gratitude to Professor Robert Whitworth for his generous help during his sabbatical at Dartmouth College. Only through his expertise were we able to produce ice samples of very high quality which were essential to the success of these experiments. We are also grateful to Mr Gary Kuehn, who provided the polycrystalline

ice. Professor E. M. Schulson is acknowledged for the use of the Ice Research Laboratory. This work is supported by the Army Research Office through grant No. DAA G29-85-K-0251. Synchrotron topography was carried out on the Stony Brook Topography Station (beamline X-19C) at the NSLS which is supported by DOE under grant No. DE-F902-84ER-45098 and in part by the donors of the Petroleum Research Fund, which is administered by the American Chemical Society.

References

1. A. HIGASHI, "Lattice Defects in Ice Crystals, X-ray Topographic Observations" (Hokkaido University Press, Sapporo, 1988).
2. T. HONDOH, K. AZUMA and A. HIGASHI, *J. Physique* **48** Colloque Cl. (1987) 183.
3. S. AHMAD and R. W. WHITWORTH, *Phil. Mag. A* **57** (1988) 749.
4. C. SHEARWOOD and R. W. WHITWORTH, *J. Glaciology* **35** (1989) 281.
5. S. AHMAD, M. OHTOMO and R. W. WHITWORTH, *J. Physique* **48** Colloque Cl. (1987) 175.
6. C. SHEARWOOD and R. W. WHITWORTH, *Phil. Mag. A* **64** (1991) 289.
7. T. HONDOH and A. HIGASHI, *J. Phys. Chem.* **87** (1983) 4044.
8. *Idem, Phil. Mag. A* **39** (1979) 137.
9. A. HIGASHI, *J. Glac.* **21** (1978) 589.
10. P. V. HOBBS, "Ice Physics" (Clarendon Press, Oxford, 1974) p. 205.
11. K. HIGUCHI, *Acta Metall.* **6** (1958) 636.
12. I. BAKER, proposal to Army Research Office (1990).
13. M. OGURO and A. HIGASHI, *Jpn J. Appl. Phys.* **18** (1979) 1897.
14. *Idem, J. Cryst. Growth* **51** (1981) 71.

Received 21 January
and accepted 7 June 1991